

Cite this:  
DOI: <https://doi.org/10.56748/ejse.234383>

Received Date: 29 March 2023  
Accepted Date: 08 June 2023

1443-9255  
<https://ejsei.com/ejse>

Copyright: © The Author(s).  
Published by Electronic Journals for  
Science and Engineering  
International (EJSEI).

This is an open access article under  
the CC BY license.

<https://creativecommons.org/licenses/by/4.0/>



# Mechanical properties test of plant fiber reinforced cementitious composites panel

Jumping He<sup>a</sup>, Zongfeng He<sup>a</sup>, Qing Cui<sup>a</sup>, Xinyuan Wang<sup>b</sup>, Xuansheng Cheng<sup>b\*</sup>

<sup>a</sup> Gansu First Construction Group Co., Ltd., Lanzhou 730070, China

<sup>b</sup> Key Laboratory of Disaster Prevention and Mitigation in Civil Engineering of Gansu Province, Lanzhou University of Technology, Lanzhou 730050, China

\* Corresponding author: chengxslut@sina.com

## Abstract

Plant fiber reinforced cementitious composites (PFRCC) panel has become the focus of current research due to their advantages of being lightweight, high strength, and good machinability. However, most scholars have studied the effects of different kinds of plant fibers on their mechanical properties, and few scholars have studied the effects of thickness changes on their mechanical properties. Therefore, a new plant fiber reinforced cementitious composites panel was developed in this paper, and the influence of thickness change on its mechanical properties was studied by axial tensile test and three-point bending test. The results show that: (1) With the increase of the thickness of the PFRCC panel, the tensile failure load increases gradually, but the peak tensile strain and tensile strength remain unchanged. The peak tensile strain is about 0.022 %, which is 1.47-2.2 times that of the matrix cement mortar. The average tensile strength is about 2.52 MPa, which is slightly higher than that of cement mortar. (2) With the increase of PFRCC panel thickness, the bending failure load increases gradually, but the bending strength remains unchanged, and the peak displacement decreases gradually. The bending strength of the PFRCC panel is about 13.5 MPa, which is 2.7 times that of the matrix cement mortar. The above research provides a theoretical basis for the application of PFRCC panels in practical engineering such as permanent formwork of foundation beams and light-gauge steel stud concrete composite external wall panels.

## Keywords

Composite material, Matrix of cement, Plant fiber, Tensile test, Three-point bending test

## 1. Introduction

At present, due to the increasing level of economic development, urban construction is also developing at a high speed. This leads to the proportion of building energy consumption in total social energy consumption increasing year by year. Therefore, building energy conservation has been an urgent problem to be solved. PFRCC panels are widely used in various engineering practices because of their high strength, moisture-proof and waterproof, flame retardant, anti-corrosion and antibacterial, good machining performance, and easy decoration. Therefore, the mechanical properties of fiber-reinforced cementitious composites have become the focus of many scholars.

The widely used fibers at home and abroad are carbon fiber, polyethylene fiber, polypropylene fiber, polyvinyl alcohol fiber (PVA), steel fiber, polypropylene fiber, plant fiber, and so on. For the above fiber cement-based materials, scholars have carried out a lot of mechanical properties research. Jamsawang et al. (2018) studied the effect of four fiber contents of seven different types of fibers on the flexural properties of fiber cement-based composites. Sarigaphuti et al. (1993) selected the plant fiber isolated from poplar and pine as the reinforcing material of concrete and found that the fiber with a volume content of 0.5% could control the crack propagation of concrete. Hasan et al. (2022) studied plant fiber-reinforced concrete's different mechanical properties, chemical properties, and environmental effects. Congro et al. (2021) proposed a new numerical model to simulate the mechanical behavior of cement-based composites in tension and bending. Ghadakpour et al. (2020) studied the effect of cement and kenaf fiber (KF) on mortar with cement content, kenaf fiber content, and length as evaluation values. Teixeira and Flávio (2020) used different lignocellulosic materials such as eucalyptus, coffee shell, and coconut shell particles to study their effects on the physical, mechanical, and durability properties of fiber concrete. Deb et al. (2020) found that increasing the fiber percentage (jute or ramie) can delay the hydration rate. Zhang et al. (2020) analyzed jute fiber's distribution and strengthening mechanism in concrete through orthogonal tests and physical and mechanical analysis and found that jute fiber could significantly improve the tension and compression ratio. Wang et al. (2018) showed that with the increase of wastepaper fiber content, due to the dissolution of carbohydrates and its hindrance to cement hydration, the setting time of cement paste containing waste paper fiber was prolonged, and waste paper fiber led to more pores in hardened paste, but it improved the toughness of cement mortar. Cao and Li (2018) proposed a new model for predicting the workability and toughness of hybrid fiber-reinforced cement-based composites by using the reinforcement index, which can be used to predict the compressive toughness, flexural toughness, and equivalent flexural strength of hybrid fiber-reinforced cement-based composites. It has wide applicability and a

good correlation with test results. Long and Wang (2021) selected Masson pine needle fiber (MPNF) to study the influence of this plant fiber on the mechanical properties of concrete and found that MPNF could improve the compressive strength, splitting strength, and fracture modulus of concrete and increase its flexibility and toughness. Balea et al. (2021) have shown that fibers can delay or prevent crack propagation, and fiber size plays an important role in the crack-bridging mechanism. Deng (2016) studied the toughening effect of 4 kinds of fiber with different content on ultra-high-performance concrete through the fracture test of 161 three-point bending beams. Abbas et al. (2018) proposed an analysis model of the compressive stress-strain relationship of fiber-reinforced concrete by considering steel fibers with different lengths and diameters. Su et al. (2017) studied the interfacial transition zone (ITZ) effect based on the single fiber pull-out test, obtained the parameters describing the fiber-matrix bond-slip behavior, and established a three-dimensional numerical model for studying the static and dynamic properties of ultra-high performance steel fiber reinforced concrete. Mendes et al. (2017) studied the effect of lignocellulose of different plant fibers on the properties of PFRCC panels and found that the chemical composition of lignocellulose raw materials seemed to have a great influence on the density of the panels.

In summary, most scholars have tried to improve the mechanical properties by adding different fibers to cement-based materials, but few scholars have studied the influence of the thickness on their mechanical properties. Therefore, this paper mainly studies the influence of thickness on the mechanical properties of the PFRCC panel through the axial tensile test and three-point bending test. At the same time, the excellent performance of the PFRCC panel was reflected by comparing its mechanical properties with the cement matrix.

## 2. Materials And Methods

### 2.1 Materials

#### 2.1.1 Cement

The hydration products of cement have a great influence on the mechanical properties of PFRCC materials, so the selection of cement composition and strength grade is very important. The cement used in this paper is ordinary 42.5 Portland cement. Its composition is shown in Table 1.

#### 2.1.2 Fly ash

The main components of fly ash are a glass microsphere, a small amount of quartz, mullite, and other crystalline substances. The main role of fly ash is reflected in the three effects of morphological effect, micro aggregate effect, and volcanic ash effect. Glass microsphere helps to improve the fluidity of the mixture by reducing the friction between cement

paste and aggregate, resulting in morphological effects and micro-aggregate effects. The pozzolanic effect refers to the secondary reaction between calcium hydroxide and the components in fly ash, which refines the internal pore structure of cement-based materials, reduces shrinkage deformation and hydration heat cracks, improves the crack resistance and impermeability of composite materials, and is beneficial to the toughness improvement of PFRCC. The basic chemical composition of the fly ash selected in this paper is shown in Table 2.

### 2.1.3 Quartz sand

The smaller the quartz sand particle size, the more significant the strain-hardening characteristics of the material, and the better the harmless dispersion ability of the crack. The basic parameters of quartz sand used in this paper are shown in Table 3.

### 2.1.4 Superplasticizer and water

The mechanism of a superplasticizer is to improve the dispersion of various material particles in the mixture, thereby reducing water consumption and improving the working performance of the mixture. The superplasticizer used in this paper is polycarboxylate superplasticizer, and its basic properties are shown in Table 4. Water is ordinary water.

### 2.1.5 Plant fiber

As shown in Fig. 1, the plant fiber selected in this paper is bamboo pulp fiber. The main performance parameters of plant fiber are shown in Table 5.



Fig. 1 Bamboo pulp fiber

Table 1 Chemical composition of cement (%)

SiO <sub>2</sub>	Al <sub>2</sub> O <sub>3</sub>	Fe <sub>2</sub> O <sub>3</sub>	CaO	MgO	SO <sub>3</sub>	K <sub>2</sub> O	Na <sub>2</sub> O	Loss
20.87	4.87	3.59	64.47	2.13	2.52	0.65	0.12	0.78

Table 2 Basic chemical composition of fly ash (%)

Composition	SiO <sub>2</sub>	Al <sub>2</sub> O <sub>3</sub>	Fe <sub>2</sub> O <sub>3</sub>	CaO	MgO	SO <sub>3</sub>	K <sub>2</sub> O	Other
Content	52	28.68	4.5	8.07	1.18	1.14	1.54	2.89

Table 3 Basic performance parameters of sand

Class	Soil content (%)	Apparent density (kg/m <sup>3</sup> )	Bulk density (kg/m <sup>3</sup> )	Porosity (%)	fineness modulus
sand	2.0	2521	1514	39.9	2.4

Table 4 Basic properties of superplasticizer

Class	pH	Water retention capacity (%)	water content (%)	specific gravity	water reducing ratio (%)
polycarboxylate superplasticizer	6	20	80	1.06	30

Table 5 Main performance parameters of bamboo fiber

Density (g/cm <sup>3</sup> )	Tensile strength /MPa	Elastic modulus /GPa	Extension at break
1.1	350	22	5.8

Table 6 Composition of the cement matrix

42.5 Cement (Kg/m <sup>3</sup> )	Fly ash (Kg/m <sup>3</sup> )	Quartz sand (Kg/m <sup>3</sup> )	Water (Kg/m <sup>3</sup> )	Superplasticizer (Kg/m <sup>3</sup> )	Water-binder ratio (W/B)
550	650	550	395	5.225	0.33

## 2.2 Experimental Investigation

### 2.2.1 Construction of the panels

As shown in Table 6, the cement matrix of plant fiber reinforced cementitious composites panels was composed of ordinary 42.5 Portland cement, fly ash, quartz sand, water, and polycarboxylate superplasticizer. The standard cube concrete samples with a size of 150mm×150mm×150mm were prepared, and the 28-day compressive strength of the cement matrix is 45.8 MPa. The plant fiber used in plant fiber reinforced cementitious composites panels was bamboo pulp fiber with an average length of about 2.04 mm, and its volume fraction was about 6%.

### 2.2.2 Experiment Investigations

#### Tensile properties

To obtain the effect of thickness on the tensile properties of PFRCC panels, axial tensile tests were carried out on PFRCC panels with four thicknesses. To prevent the specimen doesn't break from the middle part, the stress concentration occurs at the two ends due to the pressure of the fixture, and the fracture occurs from the end of the fixture, which affects the correctness of the test results. In this paper, the PFRCC panel is designed as the dumbbell-shaped specimen shown in Fig. 2 and Fig. 3.

As shown in Fig. 4, the test data were recorded independently by the universal mechanical testing machine test system. The loading speed of 10mm/min was continuously loaded until the specimen was destroyed, the tensile load was recorded, and the failure mode was observed. During the test, to prevent eccentric tension, uniform loading should be maintained. The specimen should be fixed in the middle of the two chucks of the tensile

testing machine, with a distance of about 120 mm. The specimen should be kept vertical, and the center should pass through the axis of the movable fixture of the testing machine. From the beginning of loading, the specimen was destroyed within (60±30) s, and the failure load  $F_{max}$  was recorded. The width and thickness of the tensile section were measured and averaged. The tensile strength of the specimen was calculated by Eq. (1):

$$\sigma_1 = \frac{F_{max}}{b \times t} \quad (1)$$

Where  $\sigma_1$  is tensile strength (MPa);  $F_{max}$  is failure load (N);  $b$  is the average width of the tensile section of the specimen (mm);  $t$  is the average shear surface length of the tensile section thickness of the specimen (mm).

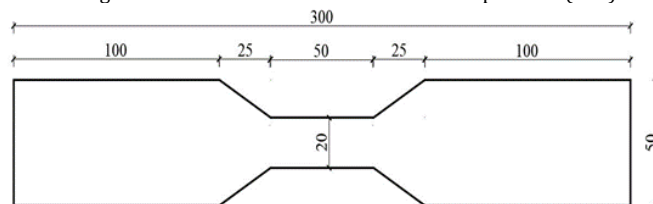


Fig. 2 Processing size of PFRCC panel axial tensile specimen

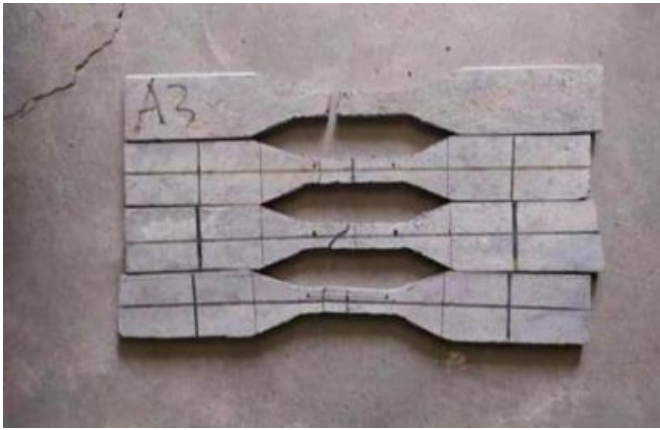


Fig. 3 Axial tensile specimen of PFRCC panel



Fig. 4 Axial tensile test of PFRCC panel

#### Bending properties

To obtain the effect of thickness on the bending properties of PFRCC panels, three-point bending tests were carried out on PFRCC panels with four thicknesses. The three-point bending test device is shown in Fig. 5 and Fig. 6. The span of the two supports at the bottom of the loading device was set to 200mm, and the size of the specimen was the length (250mm) × width (100mm). To prevent test errors, three sets of specimens were used for each thickness of the PFRCC panels.

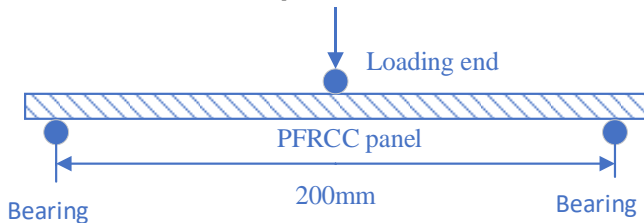


Fig. 5 Three-point bending test loading diagram.

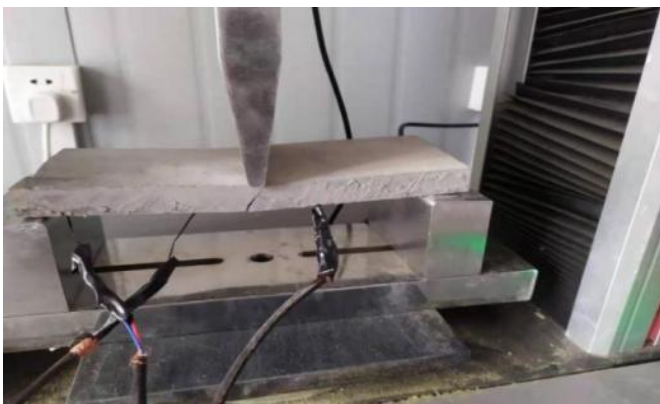


Fig. 6 Three-point flexure test

This test used static loading with a 10 mm/min loading rate. The universal mechanical testing machine automatically collected the experimental data. The specific loading steps were as follows:

(1) The specimen was placed on the bearing so that the plate's center line and the loading rod's center line coincide. The loading speed was controlled to fracture the specimen within 10s-30s, and the breaking load was read.

(2) The width of the specimen at the fracture and the thickness of the symmetrical two points were measured. The result was revised to 0.1 mm.

(3) The panel's bending strength was calculated according to Eq. (2), and the result was revised to 0.1 MPa.

$$\sigma = \frac{3PL}{2be^2} \quad (2)$$

where  $\sigma$  is bending strength (MPa);  $P$  is failure load (N);  $L$  is bearing spacing (mm);  $b$  is the width of specimen section (mm);  $e$  is specimen section thickness (mm).

### 3. Results and Discussion

#### 3.1 Axial tensile failure forms

According to the failure form of the specimen, there are two kinds of failure forms. As shown in Fig. 7, failure form 1 shows that the stress concentration occurs at the variable section and the crack is skewed, indicating that the specimen is not uniform or eccentrically stretched. The failure form of specimen 2 is broken in the middle of the equal straight section, and the crack is close to perpendicular to the axis, indicating that the specimen is uniform and the axial tension is realized. It can be seen that the defects of the specimen should be avoided as far as possible in the process of specimen making. During the axial tensile test of the PFRCC panel, the main failure form of the specimen is the main crack in the effective observation area of the specimen. Adjust the specimen, fixture, and machine joint to be in the same vertical plane before loading. Grinding the clamping area of the specimen with a file can effectively avoid the specimen being subjected to torque at the initial stage of loading and avoid damage to the specimen at the variable section.



(a) Specimen failure form 1



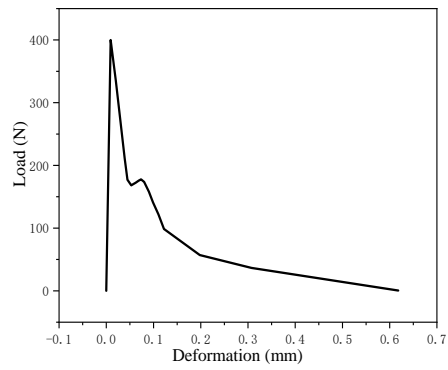
(b) Specimen failure form 2

Fig. 7 Tensile failure form diagram of PFRCC panel

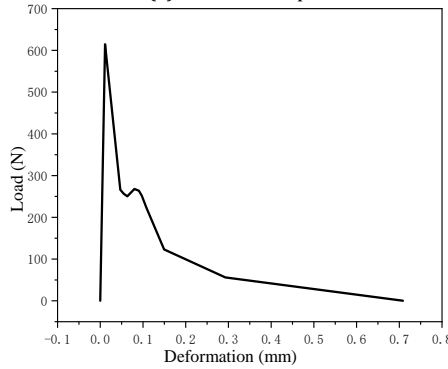
#### 3.2 Effect of thickness on tensile properties of PFRCC panel

Table 7 Axial tensile strength test results of PFRCC panels

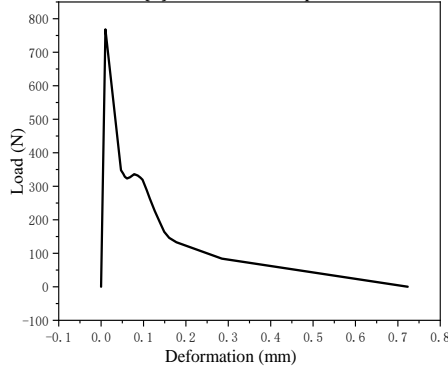
Specimen number	b×t (mm)	F <sub>max</sub> (N)	Tensile strength (MPa)
Specimen I	20×8	404.24	2.53
Specimen II	20×12	616.75	2.56
Specimen III	20×15	768.25	2.56
Specimen IV	20×18	866.99	2.41



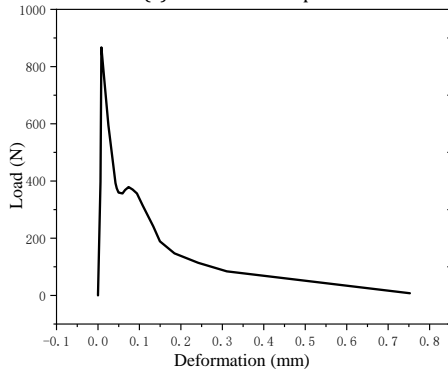
(a) 8mm PFRCC panel



(b) 12mm PFRCC panel



(c) 15mm PFRCC panel



(d) 18mm PFRCC panel

**Fig. 8 Axial tensile load-deformation curve of PFRCC panel**

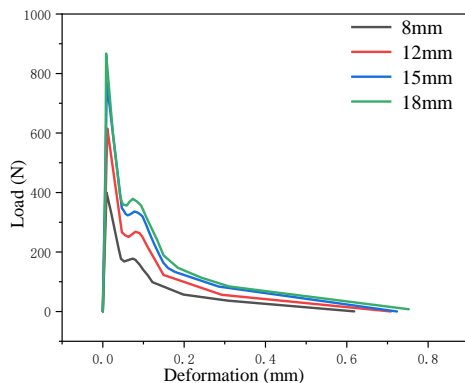


**Fig. 9 Comparison of the axial tensile load-deformation curve of the PFRCC panel**

As shown in Table 7 and Fig 8, the peak load of tensile strength failure of the 8mm PFRCC panel is 404.24N, the peak deformation is 0.009mm, and the peak tensile strain is about 0.018%. The peak tensile strength load of the 12mm PFRCC panel is 616.75N, its peak deformation is 0.011mm, and its peak tensile strain is about 0.022%. The peak load of tensile strength failure of the 15mm PFRCC panel is 768.25 N, the peak deformation is 0.010 mm, and the peak tensile strain is about 0.02%. The peak load of tensile strength failure of the 18mm PFRCC panel is 866.99 N, the peak deformation is 0.013 mm, and the peak tensile strain is about 0.026%. The peak tensile strain remains unchanged, with an average of about 0.022 %. The 28-day peak tensile strain of the matrix cement mortar is about 0.01-0.015 %, and the peak tensile strain is 1.47-2.2 times that of matrix cement mortar. Moreover, it can be seen from the load-displacement curve that after the load reaches the first peak value of the ultimate load, the bearing capacity drops sharply to a certain value. At this time, the plant fiber bridged between the cracks plays a bearing role, and the bearing capacity will rise in a small range, but the bearing capacity will rise very little, and then the bearing capacity will decrease to 0, and the specimen will fail.

It can be seen from the above that the thickness of the PFRCC panel from 8mm to 12mm is increased by 4mm, and the failure load is increased by 52.5%. The thickness of 12 mm to 15 mm increased by 3 mm, and the failure load increased by 24.6%. The thickness of 15mm to 18mm increased by 3mm, and the failure load increased by 12.8%. The average tensile strength of PFRCC panels with 8mm, 12mm, 15mm, and 18mm is 2.53 MPa, 2.56 MPa, 2.56 MPa, and 2.41 MPa respectively. The tensile strength of the PFRCC panel does not change much with the increase of PFRCC panel thickness, indicating that the tensile strength of the PFRCC panel is independent of its thickness change, and the tensile strength is about 2.52 MPa.

As shown in Fig. 9, the tensile curves of PFRCC panels with different thicknesses are compared and analyzed. The results show that the failure load of PFRCC panels increases with the increase in thickness, while the peak deformation and peak tensile strain do not change with the increase in thickness. The tensile strength curve of the PFRCC panels can be divided into three stages : (1) Elastic stage: the curve presents a linear change. In this stage, the cement matrix and fiber bear the load together, and there is no crack before reaching the peak load of curve failure. (2) Plastic stage: the first crack appears in the specimen, and the curve drops suddenly and then turns. Since then, the fiber bridging between the cracks plays a bearing role, the bearing capacity has increased, and the deformation continues to increase. The number of fluctuations on the curve represents the number of cracks. (3) Failure stage: The matrix completely loses its bearing capacity.

### 3.3 Bending failure form

The failure form of the PFRCC panel three-point bending test can be described as the load-displacement curve changing linearly at the beginning, which is usually called the elastic deformation stage. As the load continues to increase, the load-displacement curve begins to show a slow upward trend. In this section, many micro-cracks that are difficult to observe by the naked eye continue to appear in the cement matrix. When the load rises to a certain stage, it begins to fall. Currently, most of the plant fibers are pulled off, a few fibers are pulled out of the cement matrix, and the PFRCC material is damaged. The final damage is mainly concentrated at the place where the pressure of the indenter is concentrated, and the fracture surface presents a "sawtooth" shape. The failure form of the specimen is shown in Fig. 10.



**Fig. 10 Bending failure form of PFRCC pane**

### 3.4 Effect of thickness on bending properties of PFRCC panel

As shown in Table 8 and Fig. 11, the thickness of the PFRCC panel from 8mm to 12mm increased by 4mm, the average initial crack load increased by 133.1%, and the average failure load increased by 123.2%, the initial crack displacement  $\delta_1$  is reduced by 0.33 mm, the peak displacement  $\delta_m$  is reduced by 0.45 mm. The thickness of 12 mm to 15 mm increased by 3 mm, the average initial crack load increased by 73.7%, the average failure load increased by 62.9%, the initial crack displacement decreased by 0.08 mm, and the peak displacement  $\delta_m$  decreased by 0.13 mm. The thickness from 15 mm to 18 mm increased by 3 mm, the average initial crack load increased by 35.9%, the average failure load increased by 43.0%, the initial

crack displacement  $\delta_1$  decreased by 0.13 mm, and the peak displacement  $\delta_m$  decreased by 0.17 mm. The mean values of initial crack bending strength of PFRCC panels with 8mm, 12mm, 15mm, and 18mm are 11.6 MPa, 12.0 MPa, 13.4 MPa, and 12.6 MPa, respectively, and the mean values of bending strength are 13.3 MPa, 13.2 MPa, 13.8 MPa, and 13.7 MPa. The initial crack bending strength  $\sigma_1$  and the failure bending strength  $\sigma_m$  of the PFRCC panel does not change much with the increase of the thickness of the PFRCC panel, which indicates that the initial crack bending strength  $\sigma_1$  and the failure bending strength  $\sigma_m$  of the PFRCC panel has nothing to do with the thickness change, but the initial crack displacement and the peak displacement decrease with the increase of the thickness.

**Table 8 Three-point bending test results of PFRCC panel**

Thickness	Specimen number	$P_1$	$P_m$	$\delta_1$	$\delta_m$	$\sigma_1$	$\sigma_m$
8mm	A-1	245.7	285.9	1.46	1.95	11.5	13.4
	A-2	243.5	273.1	1.43	1.92	11.4	12.8
	A-3	254.9	294.4	1.38	1.84	11.9	13.8
	Mean value	248.0	284.5	1.42	1.90	11.6	13.3
12mm	B-1	559.7	633.6	1.07	1.38	11.6	13.2
	B-2	564.8	619.2	1.10	1.47	11.7	12.9
	B-3	610.2	652.8	1.12	1.50	12.7	13.6
	Mean value	578.2	635.2	1.09	1.45	12.0	13.2
15mm	C-1	1032.9	1065.0	0.98	1.38	13.8	14.2
	C-2	983.8	1012.5	1.01	1.31	13.1	13.5
	C-3	996.5	1027.5	1.03	1.28	13.2	13.7
	Mean value	1004.4	1035.0	1.01	1.32	13.4	13.8
18mm	D-1	1393.9	1468.8	0.80	1.05	12.9	13.6
	D-2	1326.7	1488.9	0.91	1.18	12.3	13.8
	D-3	1376.3	1483.3	0.95	1.23	12.7	13.7
	Mean value	1365.6	1480.3	0.88	1.15	12.6	13.7

Where  $P_1$  is cracking load,  $P_m$  is failure load,  $\delta_m$  is peak displacement,  $\delta_1$  is initial crack displacement,  $\sigma_1$  is initial crack bending strength,  $\sigma_m$  is destroyed bending strength.

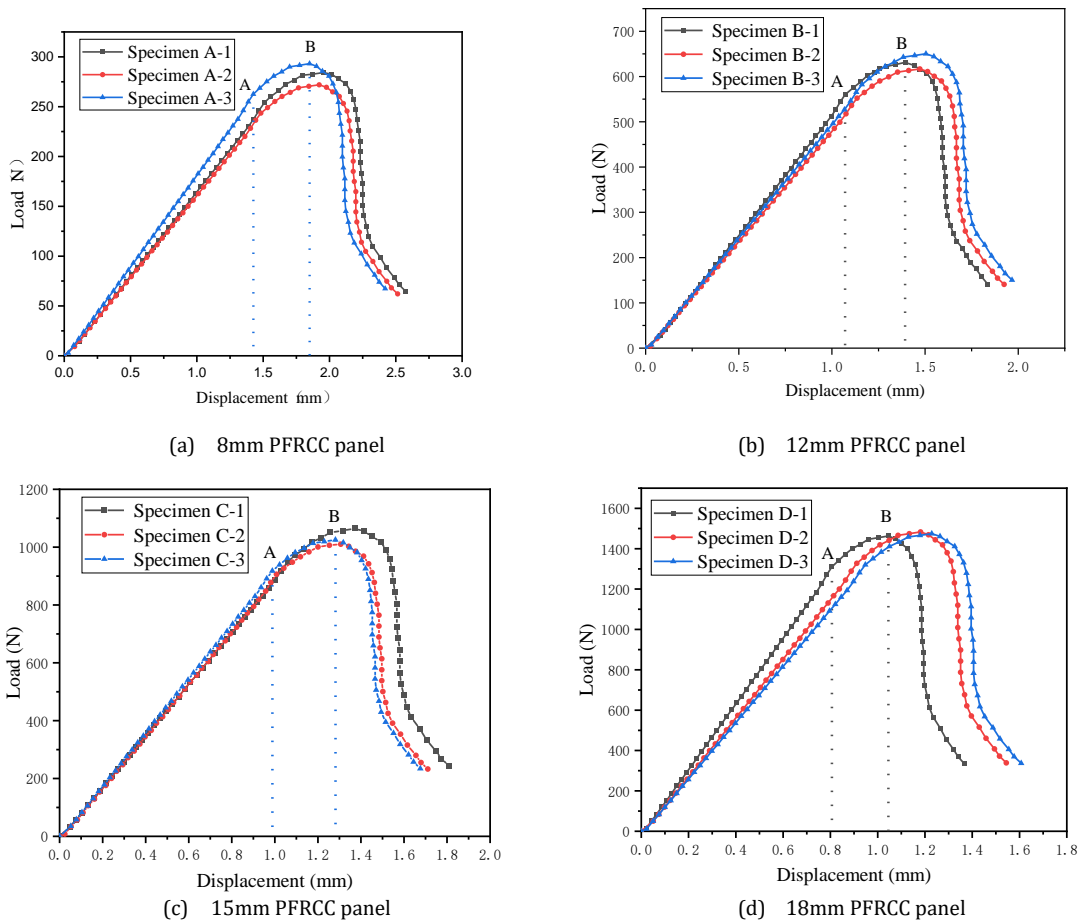


**Fig. 11 Three-point bending load-displacement curve**

As shown in Fig 9, when the PFRCC panel is subjected to a bending load, there is a straight line before point A. This stage is usually called the elastic deformation stage, and the stress corresponding to point A is called initial cracking bending strength. At point A, the first micro-crack in the cement matrix due to load appeared. And from point A, the plant fiber in the cement matrix is subjected to the action of bending tension. After leaving point A, the load-displacement curve shows a slowly rising curve segment. In this segment, with the increase of load, a large number of micro-cracks continue to appear in the cement matrix, but it is generally difficult to observe by the naked eye. At point B, most of the plant fibers are pulled off, and a small part of the fibers are pulled out from the cement matrix. At this time, the composite material is destroyed, and the stress corresponding to point B is called failure bending strength. Compared with ordinary cement-based materials, the brittleness of the PFRCC is relatively small, showing a certain toughness, while the A-B stage is called the strain hardening stage. At this stage, the upward trend of the load-displacement curve slows down, the load increases less, the deformation increases larger, and the cracks increase evenly. After point B, the PFRCC panel is in the failure stage. At this time, the bearing capacity and deformation decrease rapidly. The bearing capacity of the section with less fiber distribution reaches the maximum value first. The fracture or pull-out of plant fiber causes the crack to become larger and larger. Since then, due to stress concentration, the crack gradually expands, and the specimen breaks.

## 4. Conclusions

(1) The PFRCC panel developed in this paper is composed of mortar with compressive strength of 45.8 MPa as cement matrix and about 6% bamboo pulp fiber. With the increase in thickness, the tensile failure load increases gradually, and the peak tensile strain and tensile strength are unchanged. The tensile strength at about 2.52 MPa, which is slightly higher than that of the matrix cement mortar. The average peak tensile strain is about 0.022%, which is 2.2 times that of the matrix mortar, which proves that the addition of plant fiber increases the toughness of cement-based materials.

(2) Through the three-point bending test of the PFRCC panel, the research shows that with the increase of the thickness of the PFRCC panel, the initial cracking load and failure load will gradually increase, but the initial cracking bending strength and failure bending strength will not change. The average initial crack bending strength of the PFRCC panel is 12.4MPa, and the average failure bending strength is 13.5MPa, which is 2.7 times that of the matrix mortar. The initial crack displacement and peak displacement will decrease with the increase of its thickness.

(3) The tensile strength curve of a PFRCC panel can be divided into three stages: elastic stage, plastic stage, and failure stage. The three-point bending load-displacement curve of the PFRCC panel can be divided into three stages: elastic stage, strain hardening stage, and failure stage.

(4) Through the above axial tensile test and three-point bending test, the mechanical properties of the PFRCC panel developed in this paper are studied in detail. It is found that it has the characteristics of strong toughness and high bending strength compared with the ordinary cement mortar matrix. In the future, it will be applied to the foundation beam permanent formwork and light-gauge steel stud concrete composite external wall panels.

## Conflicts of Interest

The authors declare that there are no conflicts of interest regarding the publication of this paper.

## Data Availability

All data, models, and code generated or used during the study appear in the submitted article.

## Acknowledgments

This research is supported in part by the National Natural Science Foundation of China (Grant number: 51968045).

## References

Abbass, W., Khan, M. I., & Mourad, S. (2018). Evaluation of mechanical properties of steel fiber reinforced concrete with different strengths of concrete. *Construction and building materials*, 168, 556-569. <https://doi.org/10.1016/j.conbuildmat.2018.02.164>

Balea, A., Fuente, E., Monte, M. C., Blanco, Á., & Negro, C. (2021). Fiber reinforced cement based composites. In *Fiber Reinforced Composites* (pp. 597-648). Woodhead Publishing. Teixeira, F. P., & de Andrade Silva, F. (2020). On the use of natural curauá reinforced cement based composites

for structural applications. *Cement and Concrete Composites*, 114, 103775. <https://doi.org/10.1016/j.cemconcomp.2020.103775>

Cao, M., & Li, L. (2018). New models for predicting workability and toughness of hybrid fiber reinforced cement-based composites. *Construction and Building Materials*, 176, 618-628. <https://doi.org/10.1016/j.conbuildmat.2018.05.075>

Congro, M., Roehl, D., & Mejia, C. (2021). Mesoscale computational modeling of the mechanical behavior of cement composite materials. *Composite Structures*, 257, 113137. <https://doi.org/10.1016/j.compstruct.2020.113137>

Deng, Z. C., (2016). Flexural toughness and characterization method of hybrid fibers reinforced ultra-high performance concrete. *Acta materiae compositae sinica* 33(6): 1274-1280.

Deb, S., Mitra, N., Majumdar, S. B., & Roy, D. (2020). Rate of Hydration of Lignocellulosic Fiber-Reinforced Hydrated Cement. *ACI Materials Journal*, 117(6), 177-186.

Ghadakpour, M., Choobbasti, A. J., & Kutanaei, S. S. (2020). Investigation of the Kenaf fiber hybrid length on the properties of the cement-treated sandy soil. *Transportation Geotechnics*, 22, 100301. <https://doi.org/10.1016/j.trgeo.2019.100301>

Hasan, K. F., Horváth, P. G., & Alpár, T. (2022). Lignocellulosic fiber cement compatibility: a state of the art review. *Journal of Natural Fibers*, 19(13), 5409-5434. <https://doi.org/10.1080/15440478.2021.1875380>

Jamsawang, P., Suansomjeen, T., Sukontasukkul, P., Jongpradist, P., & Bergado, D. T. (2018). Comparative flexural performance of compacted cement-fiber-sand. *Geotextiles and Geomembranes*, 46(4), 414-425. <https://doi.org/10.1016/j.geotexmem.2018.03.008>

Long, W., & Wang, Y. (2021). Effect of pine needle fibre reinforcement on the mechanical properties of concrete. *Construction and Building Materials*, 278, 122333. <https://doi.org/10.1016/j.conbuildmat.2021.122333>

Mendes, R. F., Vilela, A. P., Farrapo, C. L., Mendes, J. F., Tonoli, G. H. D., & Mendes, L. M. (2017). Lignocellulosic residues in cement-bonded panels. In *Sustainable and nonconventional construction materials using inorganic bonded fiber composites* (pp. 3-16). Woodhead Publishing. <https://doi.org/10.1016/B978-0-08-102001-2.00001-2>

Su, Y., Li, J., Wu, C., Wu, P., Tao, M., & Li, X. (2017). Mesoscale study of steel fibre-reinforced ultra-high performance concrete under static and dynamic loads. *Materials & Design*, 116, 340-351. <https://doi.org/10.1016/j.matdes.2016.12.027>

Sargaphuti, M., Shah, S. P., & Vinson, K. D. (1993). Shrinkage cracking and durability characteristics of cellulose fiber reinforced concrete. *Materials Journal*, 90(4), 309-318.

Teixeira, F. P., & de Andrade Silva, F. (2020). On the use of natural curauá reinforced cement based composites for structural applications. *Cement and Concrete Composites*, 114, 103775. <https://doi.org/10.1016/j.cemconcomp.2020.103775>

Wang, Z., Li, H., Jiang, Z., & Chen, Q. (2018). Effect of waste paper fiber on properties of cement-based mortar and relative mechanism. *Journal of Wuhan University of Technology-Mater. Sci. Ed.*, 33(2), 419-426.

Zhang, T., Yin, Y., Gong, Y., & Wang, L. (2020). Mechanical properties of jute fiber-reinforced high-strength concrete. *Structural Concrete*, 21(2), 703-712. <https://doi.org/10.1002/suco.201900012>